

A simple model of the reflection effect for the interacting binaries and extrasolar planets

J. Budaj

Astronomical Institute, Slovak Academy of Sciences, Tatranska Lomnica 05960, Slovak Republic
budaj@ta3.sk

ABSTRACT

Extrasolar planets are a natural extension of the interacting binaries towards the companions with very small masses and similar tools might be used to study them. Unfortunately, the generally accepted treatment of the reflection effect in interacting binaries cannot be applied to very cold objects irradiated by hot objects or to extrasolar planets.

The aim of this paper is to develop a simple model of the reflection effect which could be easily incorporated into the present codes for modeling interacting binaries so that they can be used to study above mentioned objects.

Our simple model of the reflection effect takes into account the reflection (scattering), heating and heat redistribution over the surface of the irradiated object. The shape of the objects is described by the Roche potential and limb and gravity darkening can be taken into account. The orbital revolution and rotation of the planet with proper Doppler shifts for the scattered and thermal radiation are also accounted for. The new model was incorporated into the code SHELLSPEC which was originally designed for interacting binaries. Subsequently, light-curves of exoplanets (HD189733b) are modeled and the effects of the heat redistribution and limb darkening/brightening are studied.

We also calculate the exact Roche shapes of all 63 transiting extrasolar planets known so far. It is found that the departures from the sphere vary considerably within the sample. Departures of about 1% are common. About 8% of planets show departures that exceed 3% (all of them have semi-major axes smaller than 0.03 AU). In some cases (WASP-12b, WASP-19b) departures reach about 10%.

Subject headings: (stars:) binaries (including multiple): close — (stars:) binaries: eclipsing — stars: low-mass, brown dwarfs — (stars:) planetary systems

1. Introduction

There are sophisticated computer codes for calculating and inverting light curves or spectra of binary stars with various shapes or geometry including the Roche model (Lucy 1968; Wilson & Devinney 1971; Wood 1971; Mochnacki & Doughty 1972; Rucinski 1973; Hill 1979; Popper & Etzel 1981; Zhang et al. 1986; Djurasevic 1992; Drechsel et al. 1994; Linnell & Hubeny 1996; Hadrava 1997; Bradstreet & Steelman 2002; Pribulla 2004; Pavlovski et al. 2006; Tamuz et al. 2006) The Wilson & Devinney code is most often used and is continuously be-

ing improved or modified (Kallrath et al. 1998; Prša & Zwitter 2005). The reflection effect is taken into account in most of these codes.

The standard description of this effect is given in Wilson (1990). This effect is understood in the following way: A surface element of star A is irradiated by many surface elements of star B. A fraction of impinging energy called bolometric albedo (Rucinski 1969) is converted into the heat which rises the local effective temperature and re-radiates the energy on the day side of the object. An increase of the temperature on the day side of one object triggers a secondary reflection effect

on the second object and one, two or several iterations are allowed to converge to a final state. Roche model, limb darkening and gravity darkening are taken into account. This model does a good job for many interacting binaries.¹

However, there are several problems with this model which prevent its application to extrasolar planets or binaries with very different temperatures of the companions. When it comes to very cold strongly irradiated objects a considerable amount of energy might be reflected off the surface. The above mentioned reflection effect in the interacting binaries neglects this reflected light which can be essential, especially at the shorter wavelength. Well known example of such effect are the planets and moons in our Solar system in the visible light. This reflected light bears the spectroscopic signatures of the hot irradiating star and is not converted into the heat and re-radiated. The definition of the albedo in the planetary sciences is almost the opposite of its meaning in the interacting binaries. Here, the albedo is a fraction of the impinging energy which is reflected off the object and is not absorbed and converted into the heat. Reflected and re-radiated photons may also have completely different Doppler shifts depending on the mutual velocities of the two objects and observer.

Moreover, some portion of the energy absorbed on the day side can be transferred to and irradiated from the night side. Calculations of atmosphere models of extrasolar planets (Hubeny et al. 2003; Barman et al. 2005; Burrows et al. 2008; Fortney et al. 2008) demonstrate that there is a deep temperature plateau which turns off the convection in the atmospheres. Convection and vertical energy transport operates only at very deep layers. On the other hand, hydrodynamical simulations (Dobbs-Dixon & Lin 2008; Showman et al. 2009; Menou & Rauscher 2009) of the atmospheres of extrasolar planets indicate that there are very strong horizontal currents and jets which can effectively redistribute and circulate the energy between the day and night side of the planet especially along the lines of constant latitudes.

¹ One might point out that the name "reflection effect" is misleading in this context since the effect as it is described above has nothing to do with the reflection (process of light scattering) and it deals only with the heating and re-radiating.

At the same time, many transiting exoplanets are so close to their host stars that their shape may depart from the sphere and be best described by the Roche model. The above mentioned effects and findings must be taken into account when modeling very cold components of interacting binaries and extrasolar planets.

The main purpose of this paper is to develop a new simple model of the reflection effect which would consider the reflected (scattered) light, heating (absorption of the light), and heat redistribution over the surface and which could be used to model the cold components of interacting binaries and extrasolar planets. The model was included into our code SHELLSPEC (Budaj & Richards 2004). This program was originally designed to calculate light-curves, spectra and images of interacting binaries immersed in a moving circumstellar environment which is optically thin. The code is freely available and might be used to study various effects observed or expected in the extrasolar planets. A Fortran90 version of the code which also solves the inverse problem was created by Tkachenko et al. (2010).

2. Roche model

In the SHELLSPEC code the Roche model serves as a boundary condition for the radiative transfer in the circumstellar matter. Both objects, star and companion, may have shapes according to the Roche model for detached or contact systems. Descriptions of the Roche model can be found in Kopal (1959), Plavec & Kratochvil (1964), and many other papers and books. Let us assume a Cartesian coordinate system (x,y,z) centered on one of the stars (labeled as 1) such that the companion (labeled as 2) is at (1,0,0) and revolves around the z axis in the direction of positive y axis. Let the mass ratio, q , always be m_2/m_1 or 'companion/star' and $q < 1$ will indicate the companion is lighter while $q > 1$ means the central star is lighter. Then, the normalized Roche potential, C , is expressed as:

$$C(x, y, z) = \frac{2}{(1+q)r_1} + \frac{2q}{(1+q)r_2} + \left(x - \frac{q}{1+q}\right)^2 + y^2 \quad (1)$$

where

$$\begin{aligned} r_1 &= \sqrt{x^2 + y^2 + z^2} \\ r_2 &= \sqrt{(x-1)^2 + y^2 + z^2}. \end{aligned} \quad (2)$$

The Roche surface of a detached component is defined as an equipotential surface $C_s = C(x_s, y_s, z_s)$ passing through the sub-stellar point (x_s, y_s, z_s) (point on the surface of the star in between the stars, $0 < x_s < 1, y_s = z_s = 0$) which is localized by the ‘fill-in’ parameter $f_i \leq 1$. We define this by:

$$f_i = x_s/L_{1x}, \quad f_i = (1 - x_s)/(1 - L_{1x}) \quad (3)$$

for the primary and the secondary, respectively. L_{1x} is the x coordinate of the L1 point $L1(L_{1x}, 0, 0)$.

Derivatives of the Roche potential are:

$$C_x = \frac{\partial C}{\partial x}, \quad C_y = \frac{\partial C}{\partial y}, \quad C_z = \frac{\partial C}{\partial z} \quad (4)$$

Gravity darkening of the non spherical objects is taken into account by varying the surface temperature according to the von Zeipel’s law:

$$T/T_p = (g/g_p)^\beta \quad (5)$$

where g is the normalized surface gravity, β is the gravity darkening coefficient, T_p, g_p are the temperature and gravity at the rotation pole. The normalized gravity vector is $\mathbf{g} = (C_x, C_y, C_z)$ and:

$$g = \sqrt{C_x^2 + C_y^2 + C_z^2}. \quad (6)$$

Notice, that there is an imminent singularity in the calculations in the vicinity of L1, L2 points since gravity falls to zero which drags temperatures (a denominator in many equations) to zero. We avoid the problem by setting the lowest possible value of $g/g_p = 10^{-4}$.

Limb darkening is taken into account using the quadratic limb darkening law:

$$I(\theta) = I(0)f_{LD} \quad (7)$$

$$f_{LD} = 1 - u_1(1 - \cos\theta) - u_2(1 - \cos\theta)^2 \quad (8)$$

and by calculating the cosine of the angle θ between the line of sight unit vector $\mathbf{n} = (n_x, n_y, n_z)$ and a normal to the surface:

$$\cos\theta = -\mathbf{n} \cdot \mathbf{g} / g = -\frac{n_x C_x + n_y C_y + n_z C_z}{\sqrt{C_x^2 + C_y^2 + C_z^2}}. \quad (9)$$

3. Irradiation and heat redistribution

In this section we will describe our treatment of the mutual irradiation of the objects. It can be applied to both objects but we will neglect multiple reflections between the two objects since this is not essential if one of them is much less luminous. We will distinguish between three separate processes: **reflection** of the light off the object (or scattering which does not produce any heating of the irradiated surface); **heating** of the irradiated surface (day side) by the absorbed light; and subsequent **heat redistribution** over the entire surface of the object. Let’s assume that the day side of a planet is irradiated by the star then the impinging flux at a location \mathbf{r} from star at \mathbf{r}_* is:

$$F_{ir} = \cos\delta \frac{R_*^2}{(\mathbf{r} - \mathbf{r}_*)^2} \sigma T_*^4 \quad (10)$$

where R_*, T_* are radius and effective temperature of the star, δ is an irradiating angle which is the zenith distance of the center of the star as seen from the surface of the planet:

$$\begin{aligned} \cos\delta &= \frac{(\mathbf{r} - \mathbf{r}_*) \cdot \mathbf{g}}{|\mathbf{r} - \mathbf{r}_*| g} = \\ &= \frac{(r_x - r_{x*})C_x + (r_y - r_{y*})C_y + (r_z - r_{z*})C_z}{|\mathbf{r} - \mathbf{r}_*| \sqrt{C_x^2 + C_y^2 + C_z^2}}. \end{aligned} \quad (11)$$

Now, let’s define two local parameters $A_B(\alpha, \beta)$, $P_r(\alpha, \beta)$ on the day side of the planet (irradiated side of an object) where α, β are the longitude and latitude, respectively measured from the sub-stellar point. A_B will be the local Bond albedo of the surface, consequently $A_B F_{ir}$ is flux immediately reflected off the surface, $(1 - A_B)F_{ir}$ will be a fraction of the irradiating energy which is converted into the heat, $P_r(1 - A_B)F_{ir}$ will be a part of the latter which is redistributed over the day and night side of the object, while the remaining part, $(1 - P_r)(1 - A_B)F_{ir}$, will heat the local area.² Then the energy conservation for the day-night heat transport can be written as:

$$\iint P_r(1 - A_B)F_{ir} dS_{day} = \iint \sigma T_{dn}^4 dS_{day+night} \quad (12)$$

²Note that local P_r is analogous but not the same as the global P_n parameter of Burrows et al. (2006), $P_n \approx P_r(1 - A_B)/2$.

Let's assume, of simplicity (or in the absence of a better approximation), that $A_B(\alpha, \beta)$, $P_r(\alpha, \beta)$ are constant and the heat is homogeneously redistributed over the day and night sides so that the surface has a constant temperature T_0 . Then,

$$P_r(1 - A_B) \iint F_{ir} dS_{day} / \iint dS_{day+night} = \sigma T_0^4. \quad (13)$$

In case the planet has a spherical shape and is far from the star this reduces to:

$$T_0^4 = \frac{1}{4} P_r (1 - A_B) \frac{R_\star^2}{d^2} T_\star^4. \quad (14)$$

Let's explore another case, namely that the horizontal circulation on the planet along the lines of constant latitude is so strong that it dominates the day-night heat transport and the equilibrium surface temperature, T_1 , will be a function of latitude. In this case and the assumptions above (spherical planet far from the star), one can consider an energy conservation for a fixed latitude:

$$P_r(1 - A_B) \int F_{ir} \cos(\beta) d\alpha = \sigma T_1^4(\beta) \int \cos(\beta) d\alpha \quad (15)$$

where

$$\cos(\delta) = \cos(\alpha) \cos(\beta). \quad (16)$$

The solution is that the temperature depends on the fourth root of $\cos(\beta)$:

$$T_1^4(\beta) = \frac{1}{\pi} P_r (1 - A_B) \frac{R_\star^2}{d^2} T_\star^4 \cos(\beta) = \frac{4}{\pi} T_0^4 \cos(\beta). \quad (17)$$

The study of these two extreme cases lead us to suggest a heat redistribution model in which the day-night heat transport is a linear combination of the two cases mentioned above. Namely, we will express the surface temperature in the following way:

$$T_{dn}^4(\beta) = T_0^4 [P_a + P_b \cos(\beta)] \quad (18)$$

where P_a, P_b are the temperature distribution parameters. $P_a = \langle 0, 1 \rangle$ and P_b is to be determined from Eq.12 so that the total energy budget is conserved. From Eq. 12,13 and 18 we obtain:

$$P_b = (1 - P_a) \frac{\iint dS_{day+night}}{\iint \cos \beta dS_{day+night}}. \quad (19)$$

It can be shown that in case of a spherical planet far from the star

$$P_b = \frac{4}{\pi} (1 - P_a) \quad (20)$$

and $P_b = \langle 0, 4/\pi \rangle$. Notice, that P_a is a measure of the effectiveness of the homogeneous temperature distribution over the surface versus the zonal distribution. It is intimately linked with the effectiveness of the heat flows along the meridians versus parallels.

Finally, the temperature distribution on the surface of the irradiated planet will be:

$$T^4 = T_{ir}^4 + T_{dn}^4 + T_{old}^4 \quad (21)$$

where $T_{ir}^4 = (1 - P_r)(1 - A_B)F_{ir}/\sigma$ on the day side, $T_{ir}^4 = 0$ on the night side, and T_{old} is the prior temperature distribution over the surface in the absence of the irradiation (including the gravity darkening etc.).

Once we know the temperature distribution over the surface, one can approximate the monochromatic flux from the surface as being composed of two parts:

$$F_\nu = F_\nu^{reflect} + F_\nu^{thermal} \quad (22)$$

Reflection depends on the surface albedo A_ν and has to take into account the mutual velocities:

$$F_\nu^{reflect} = A_{\nu 2} F_{\nu 1 ir} \quad (23)$$

$$F_{\nu 1 ir} = \cos \delta \frac{R_\star^2}{(\mathbf{r} - \mathbf{r}_\star)^2} F_{\nu 1}^\star \quad (24)$$

where $F_{\nu 1}^\star$ is properly shifted flux emerging from the surface of the irradiating star. The Doppler shifts are the following

$$\nu_2 = \nu \left(1 - \frac{v_z}{c} \right) \quad (25)$$

$$\nu_1 = \nu \left(1 - \frac{v_z + v_2}{c} \right) \quad (26)$$

$$v_2 = - \frac{(\mathbf{r} - \mathbf{r}_\star) \cdot (\mathbf{v} - \mathbf{v}_\star)}{|\mathbf{r} - \mathbf{r}_\star|} \quad (27)$$

where \mathbf{v} is the velocity field vector at the given point on the irradiated surface specified by the vector \mathbf{r} , \mathbf{v}_\star is the velocity of the center of mass of the irradiating star, and z coordinate points to the observer. To calculate the reflected intensity we assume that the reflection is isotropic in which case:

$$I_\nu^{reflect} = F_\nu^{reflect} / \pi. \quad (28)$$

Finally, $F_\nu^{thermal}$ can be approximated by the flux emerging from the non-irradiated model atmosphere with the effective temperature equal to the

surface temperature of the irradiated object given by Eq.21.

$$F_{\nu}^{thermal} = F_{\nu_2}(T_{eff} = T) \quad (29)$$

and the associated intensity is given by:

$$I_{\nu}^{thermal} = I_{\nu}(0)^{thermal} f_{LD} \quad (30)$$

$$I_{\nu}(0)^{thermal} = \frac{F_{\nu}^{thermal}}{\pi(1 - u_1/3 - u_2/6)} \quad (31)$$

In this way we fully include into account the mutual velocities of the objects and observer, the rotation of the reflecting object, its limb darkening but neglect the rotation of the irradiating object. In some cases the later can be easily taken into account by feeding the code with the precalculated rotationally broadened spectrum F_{ν}^* .

Local Bond albedo used here is a weighted monochromatic albedo A_{ν} :

$$A_B = \frac{\int A_{\nu} F_{\nu}^* d\nu}{\int F_{\nu}^* d\nu}. \quad (32)$$

One has to keep in mind that our albedos refer to the reflected light only (not to the absorbed and re-radiated light). In case the irradiated object is very cold compared to the irradiating object there is a clear distinction between its thermal radiation and reflected radiation. However, if the two objects have comparable temperatures it is almost impossible to distinguish whether a particular photon was scattered or absorbed and re-radiated. In this case it is still possible to use our formalism and e.g. approximate the albedo by the single scattering albedo to cope with the problem.

4. Application to extrasolar planets

Extrasolar planets are an attractive test-bed for such models. They are a natural extension of the interacting binaries towards cool and small mass companions. Their radiation is governed by the stellar insolation. Very sophisticated atmosphere models of exoplanets are being developed (Hubeny et al. 2003; Barman et al. 2005; Burrows et al. 2008; Fortney et al. 2008). At the same time, models with various simplifications are often very useful to study various effects (Hansen 2008; Kipping & Tinetti 2009; Madhusudhan & Seager 2009; Cowan & Agol 2010).

4.1. Shapes of the transiting extrasolar planets

Our knowledge about the size of exoplanets comes mainly from the observations of transits. A majority exoplanet studies assume that the exoplanets have a spherical shape. The precision of the photometric measurements is advancing revealing more and more details. Recently, Kipping & Tinetti (2009) attempted to model the light curve and transit assuming the spherical shape but taking into account the intrinsic night side emission of the planet during the transit. They found that in the infrared region the effect is of the order of 10^{-4} . Seager & Hui (2002), Barnes & Fortney (2003), Carter & Winn (2009) assumed the shape of the rotational ellipsoid. Welsh et al. (2010) used the Roche potential approximation to describe the shape of the parent star and to explain the ellipsoidal variations of HAT-P-7. Nevertheless, many transiting exoplanets are so close to their host stars that their shape is best described by the Roche model.

Our code was applied to transiting extrasolar planets and exact Roche model shape of all the transiting exoplanets was calculated. Circular orbit with the radius equal to the semi-major axis and synchronized rotation of the planet was assumed. The results are displayed in the Table 1. It lists R_{sub} , R_{back} , R_{pole} , R_{side} which are the radii at the sub-stellar point, anti-stellar point, rotation pole and on the side, respectively. Departures from the sphere are measured by the value of the R_{sub}/R_{pole} .

One can see that the departures from the spherical shape vary by several orders of magnitude. Departures of about 1% are common. About 8% of planets (all of them have semi-major axis smaller than 0.03 AU) have departures larger than 3%. These include: OGLE-TR-56b, WASP-4b, and CoRoT-1b. The extreme cases are WASP-12b and WASP-19b when the departures can exceed 10% or 9%, respectively. This is clearly comparable to the precision of the planet radius determination or the transit radius effect. Moreover, this shape distortion would be even higher if one was to consider the eccentricity of the orbit and assume the periastron distance instead of the semi-major axis. The highest departures seems to be along the line joining the objects (the R_{sub}/R_{pole}

parameter) which would affect mainly the overall light-curve. During the transit event, it is mainly R_{side}/R_{pole} parameter which is most relevant and this does not acquire such high values (about 2% in case of WASP-12b and WASP-19b). Nevertheless, one has to keep it in mind when interpreting the planet radius measurements or calculations (Burrows et al. 2007; Fortney et al. 2007).

4.2. Light curves of the transiting extrasolar planets

In this section, we apply our model to the light-curve of the extrasolar planet HD189733b. The planet properties were determined by Winn et al. (2007). Knutson et al. (2007) obtained the light curve of the planet which covers more than half of the orbit. It was observed at 8 micron in the infrared region.

First, let us introduce the qualitative distribution of the temperature over the surface of the planet produced by our model. Fig.1 illustrates the behaviour of the temperature for a relatively intense heat redistribution factor $P_r = 0.6$ and quite small temperature distribution parameter $P_a = 0.1$ (i.e. intense flows along parallels but not very intense heat flows along meridians). One can observe that this model produces hotter regions at the sub-stellar point and near the equator while cooler regions are at the poles. Fig.2 then illustrates the behaviour of the intensity. This is what would an observer see looking on the planet pole-on. Limb darkening was applied to the model. One would see the dark polar regions, however, the hot sub-stellar point would not be the brightest since all hotter equatorial regions would be dim due to the limb darkening. Black body approximation is used to model the energy distribution.

Now, we can proceed to a comparison between the observations of Knutson et al. (2007) and models produced by SHELLSPEC shown in Fig.3. The synthetic light-curves are very sensitive to the heat redistribution parameter $P_r = < 0, 1 >$. Especially, at the phases close to the transit, when the night side of the planet is seen, the flux can change by the orders of magnitude. The best fit is obtained for $P_r = 0.5 - 0.8$, which means that the surface heat redistribution is crucial and quite effective. It is in agreement with the findings of Knutson et al. (2007), Burrows et al. (2008), Madhusudhan & Seager

(2009), and Cowan & Agol (2010).

It is interesting to see that these kinds of light curves of transiting exoplanets are not very sensitive to the temperature distribution parameter $P_a = < 0, 1 >$ associated with the effectiveness of the homogeneous heat transfer versus zonal transfer. It is illustrated in Fig.4. If the heat flows mainly along the equator and not along the meridians ($P_a = 0$) and we view the planet almost edge-on then we observe a slight increase of flux at all phases, especially on the night side (compared to the homogeneous temperature distribution, $P_a = 1$).

It is also interesting to observe a moderate effect of the limb darkening on such light-curves of transiting exoplanets. Limb darkening is manifested mainly shortly before and after the transit and near the secondary eclipse. See Fig.5 with the comments and the description.

However, there are cases when the temperature distribution parameter, P_a , and limb darkening will be much more important. Fig.6 illustrates the situation for a hypothetical planet at an inclination of 20 degrees. We used the parameters for the non-transiting extrasolar planet HD179949b (Tinney et al. 2001) to feed the code with real numbers. However, inclination is not known for non-transiting exoplanets. In this case the effects of the temperature distribution parameter and limb darkening are indeed important and are comparable to the amplitude of the light curve. This justifies the complexity of our model with the heat and temperature distribution, and limb darkening parameters. Gravity darkening is also included but this will not be an issue for the extrasolar planets. If they are close to the star then their intrinsic radiation is negligible compared to the heavy external irradiation and if they are far from the star then their shape will be almost spherical (neglecting the rotation) and without the gravity darkening.

5. Conclusions - Summary

We argue that a new model for the reflection effect in the interacting binaries is necessary to describe properly the radiation from the cool object irradiated by the hot object. Subsequently, we proposed a new model for the reflection effect and applied it to an extreme case of an interacting

binary - extrasolar planet.

The new model introduces several free parameters. (1) Bond albedo $A_B = \langle 0, 1 \rangle$ which controls how much energy is reflected and how much is converted into the heat. $A_B = 1$ means that all impinging energy is reflected off the surface and nothing gets converted into the heat. (2) Heat redistribution parameter $P_r = \langle 0, 1 \rangle$ which controls how much heat from a certain point is redistributed to other places and how much is re-radiated locally. $P_r = 0$ means that all absorbed heat is re-radiated locally and nothing gets transported to other places. (3) Temperature distribution parameter $P_a = \langle 0, 1 \rangle$ is a measure of the effectiveness of the homogeneous heat redistribution over the surface versus the zonal distribution. $P_a = 1$ means that the heat is homogeneously redistributed over the surface while $P_a = 0$ means that the heat flows only along the lines of constant latitude. Our model properly describes the shapes of the objects by means of the Roche potential and takes into account gravity and limb darkening. At the same time it takes into account the orbital revolution, rotation and proper Doppler shifts in the scattered and thermal radiation.

It is demonstrated that the light-curves of transiting extrasolar planets are mainly sensitive to the heat redistribution parameter P_r and not so sensitive to the temperature distribution parameter P_a or to the limb darkening. However, light-curves of planets seen at very low inclinations are very sensitive also to the temperature distribution parameter P_a and limb darkening.

We calculated the exact Roche shapes of all currently known transiting exoplanets (Schneider 1995) and found out that the departures from spherical symmetry may vary significantly. Departures of the order of 1% are common, and can reach about 10% in most extreme cases like WASP-12b and WASP-19b. About 8% of transiting planets have departures more than 3% (all have semi-major axes smaller than 0.03 AU),

The author acknowledges the support from the Marie Curie International Reintegration grant FP7-200297 and partial support from the VEGA grants 2/0078/10, 2/0074/09.

REFERENCES

- Alonso, R. et al. 2004, *ApJ*, 613, L153
- Alonso, R. et al. 2008, *A&A*, 482, L21
- Anderson, D.R. et al. 2010, *ApJ*, 709, 159
- Bakos, G. et al. 2007a, *ApJ*, 671, L173
- Bakos, G. et al. 2007b, *ApJ*, 656, 552
- Bakos, G. et al. 2009a, *ApJ*, 707, 446
- Bakos, G. et al. 2009b, *ApJ*, 696, 1950
- Bakos, G. et al. 2009c, arXiv:0901.0282
- Barge, P. et al. 2008, *A&A*, 482, L17
- Barman, T.S., Hauschildt, P.H., & Allard, F. 2005, *ApJ*, 632, 1132
- Barnes, J.W., & Fortney, J.J. 2003, *ApJ*, 588, 545
- Bean, J.L. et al. 2008, *A&A*, 486, 1039
- Bouchy, F. et al. 2005, *A&A*, 444, L15
- Bradstreet, D.H., & Steelman, D.P. 2002, *BAAS*, 34, 1224
- Budaj, J., & Richards M.T. 2004, *Contrib. Astron. Obs. Skalnaté Pleso*, 34, 167
- Burke, C. et al. 2007, *ApJ*, 671, 2115
- Burke, C. et al. 2008, *ApJ*, 686, 1331
- Burrows, A., Budaj, J., & Hubeny, I. 2008, *ApJ*, 678, 1436
- Burrows, A., Hubeny, I., Budaj, J., & Hubbard, W. B. 2007, *ApJ*, 661, 502
- Burrows, A., Sudarsky, D., & Hubeny I. 2006, *ApJ*, 650, 1140
- Carter, J.A., & Winn, J.N. 2009, arXiv:0912.1594
- Charbonneau, D. et al., 2009, *Nature*, 462, 891
- Collier Cameron, A. et al. 2007, *MNRAS*, 380, 1230
- Cowan, N.B., & Agol, E. 2010, arXiv:1001.0012
- Daemgen, S., Hormuth, F., Brandner, W., Bergfors, C., Janson, M., Hippler, S., & Henning, T. 2009, *A&A*, 498, 567

- Deleuil, M. et al. 2008, *A&A*, 491, 889
- Djurasevic, G. 1992, *Ap&SS*, 197, 17
- Dobbs-Dixon, I., & Lin, D. N. C. 2008, *ApJ*, 673, 513
- Drechsel, H., Haas, S., Lorenz, R., & Mayer, P. 1994, *A&A*, 284, 853
- Fortney, J.J., Lodders, K., Marley, M.S., & Freedman, R.S. 2008, *ApJ*, 678, 1419
- Fortney, J.J., Marley, M.S., & Barnes, J.W. 2007, *ApJ*, 659, 1661
- Fossey, S.J., Waldmann, I.P., & Kipping, D.M. 2009, *MNRAS*, 396, L16
- Fridlund, M. et al. 2010, arXiv:1001.1426
- Gibson, N.P. et al. 2008, *A&A*, 492, 603
- Gillon, M., Pont, F., Moutou, C., Bouchy, F., Courbin, F., Sohy, S., & Magain, P. 2006, *A&A*, 459, 249
- Gillon, M. et al. 2007, *A&A*, 466, 743
- Gillon, M. et al. 2009, *A&A*, 501, 785
- Hadrava, P. 1997, *A&AS*, 122, 581
- Hansen, B.M.S. 2008, *ApJS*, 179, 484
- Hartman, J.D. et al. 2009, *ApJ*, 706, 785
- Hebb, L. et al. 2009, *ApJ*, 693, 1920
- Hebb, L. et al. 2010, *ApJ*, 708, 224
- Hellier, C. et al. 2009, *ApJ*, 690, L89
- Henry, G.W., Marcy, G.W., Butler, R.P., & Vogt, S.S. 2000, *ApJ*, 529, L41
- Hill, G. 1979, *Publ. Dom. Ap. Obs. Victoria* 15, 297
- Hubeny, I., Burrows, A., & Sudarsky, D. 2003, *ApJ*, 594, 1011
- Johnson, J.A., Winn, J.N., Cabrera, N.E., & Carter, J.A. 2009, *ApJ*, 692, L100
- Johns-Krull, C. et al. 2008, *ApJ*, 677, 657
- Joshi, Y.C. et al. 2008, *MNRAS*, 392, 1532
- Kallrath, J., Milone, E.F., Terrell, D., & Young, A.T. 1998, *ApJ*, 508, 308
- Kipping, D.M., & Tinetti, G. 2009, arXiv:0912.1133
- Knutson, H. et al. 2007, *Nature*, 447, 183
- Kopal, Z. 1959, *Close Binary Systems*, London, Chapman & Hall Ltd.
- Kovacs, G. et al. 2007, *ApJ*, 670, L41
- Latham, D.W. et al. 2009, *ApJ*, 704, 1107
- L'eger A. et al. 2009, *A&A*, 506, 287
- Linnell, A.P., & Hubeny, I. 1996, *ApJ*, 471, 958
- Lister, T.A. et al. 2009, *ApJ*, 703, 752
- Lucy, L.B. 1968, *ApJ*, 153, 877
- Madhusudhan, N., & Seager, S. 2009, *ApJ*, 707, 24
- McCullough, P.R. et al. 2006, *ApJ*, 648, 1228
- McCullough, P.R. et al. 2008, arXiv:0805.2921
- Menou, K., & Rauscher, E. 2009, *ApJ*, 700, 887
- Mochnacki, S.W., & Doughty, N.A. 1972, *MNRAS* 156, 51
- Moutou, C. et al. 2008, *A&A*, 488, L47
- Noyes, R.W. et al. 2008, *ApJ*, 673, L79
- O'Donovan, F.T. et al. 2007, *ApJ*, 663, L37
- Pál, A. et al. 2009, *MNRAS*, 401, 2665
- Pavlovski, K., Burki, G., & Mimica, P. 2006, *A&A*, 454, 855
- Plavec, M., & Kratochvil, P. 1964, *Bull. Astron. Inst. Czechoslovakia*, 15, 165
- Pont, F., Bouchy, F., Queloz, D., Santos, N.C., Melo, C., Mayor, M., & Udry S. 2004, *A&A*, 426, L15
- Pont, F. et al. 2007, *A&A*, 465, 1069
- Pont, F. et al. 2008, *A&A*, 487, 749
- Popper, D.M., & Etzel, P.B. 1981, *AJ*, 86, 102

- Pribulla, T. 2004, in Spectroscopically and Spatially Resolving the Components of Close Binary Stars, R.W. Hilditch et al. (eds.), ASP Conf. Series., 318, 117
- Prša, A., & Zwitter, T. 2005, ApJ, 628, 426
- Rauer, H. et al. A&A, 506, 281
- Rucinski, S.M. 1969, Acta Astronomica, 19, 245
- Rucinski, S.M. 1973, Acta Astronomica, 23, 79
- Sahu, K.C. et al. 2006, Nature, 443, 534
- Sato, B. et al. 2005, ApJ, 633, 465
- Schneider, J., 1995, The Extrasolar Planets Encyclopaedia, <http://exoplanet.eu>
- Seager, S., & Hui, L. 2002, ApJ, 574, 1004
- Showman, A.P., Fortney, J.J., Lian, Y., Marley, M.S., Freedman, R.S., Knutson, H.A., & Charbonneau, D. 2009, ApJ, 699, 564
- Shporer, A. et al. 2009, ApJ, 690, 1393
- Skillen, I. et al. 2009, A&A, 502, 391
- Smith, A.M.S. et al. 2009, MNRAS, 398, 1827
- Southworth, J. et al. 2009a, ApJ, 707, 167
- Southworth, J. et al. 2009b, MNRAS, 399, 287
- Southworth, J. et al. 2009c, MNRAS, 396, 1023
- Tamuz, O., Mazeh, T., & North, P. 2006, MNRAS, 367, 1521
- Tkachenko, A., Lehmann, H., & Mkrtichian, D. 2010, AJ, 139, 1327
- Tinney, C. G., Butler, R.P., Marcy, G.W., Jones, H.R.A., Penny, A.J., Vogt, S.S., Apps, K., & Henry, G.W. 2001, ApJ, 551, 507
- Torres, G. et al. 2007, ApJ, 666, L121
- Udalski. A. et al. 2008, A&A, 482, 299
- Weldrake, D.T.F., Bayliss, D.D.R., Sackett, P.D., Tingley, B.W., Gillon, M., & Setiawan, J. 2008, ApJ, 675, L37
- Welsh, W.F., Orosz, J.A., Seager, S., Fortney, J.J., Jenkins, J., Rowe, J.F., Koch, D., & Borucki, W.J. 2010, arXiv:1001.0413
- West, R.G. et al. 2009, AJ, 137, 4834
- Wilson, R.E., & Devinney, E.J. 1971, ApJ 166, 605
- Wilson, R.E. 1990, ApJ, 356, 613
- Winn, J.N. et al. 2007, AJ, 133, 1828
- Winn, J.N. et al. 2009, ApJ, 693, 794
- Wood, D.B. 1971, AJ, 76, 701
- Zhang, E.-H., Robinson, E.L., & Nather, R.E. 1986, ApJ, 305, 740

Table 1: Shapes of the transiting exoplanets. $(0,0,0)$ -coordinates of the center of mass of the planet. a -semi-major axis in [AU], q -star/planet mass ratio, R_{sub} -planet radius at the sub-stellar point ($R_{sub},0,0$) (assumed equal to the planet radius determined from the transit), R_{back} -planet radius at the anti-stellar point, R_{pole} -planet radius at the rotation pole $(0,0,R_{pole})$, R_{side} -planet radius at the side point $(0,R_{side},0)$, $rr = R_{sub}/R_{pole}$ -departure from the sphere, $f_i = R_{sub}/L_{1x}$ -fill-in parameter of the Roche lobe. Radii are in units of Jupiter radius.

name	a	q	Rsub	Rback	Rpole	Rside	rr	f_i	Reference
GJ 1214b	0.01400	9186.0	0.2415	0.24148	0.23904	0.23964	1.01028	0.251	Charbonneau et al. (2009)
WASP-19b	0.01640	865.2	1.3100	1.30443	1.19721	1.21965	1.09421	0.538	Hebb et al. (2010)
CoRoT-7b	0.01720	64503.6	0.1500	0.14999	0.14862	0.14895	1.00931	0.242	L'eger et al. (2009)
WASP-18b	0.02047	128.6	1.1650	1.16483	1.15892	1.16041	1.00524	0.208	Southworth et al. (2009a)
OGLE-TR-56b	0.02250	949.9	1.3000	1.29848	1.25022	1.26145	1.03982	0.401	Pont et al. (2007)
TrES-3	0.02260	504.0	1.2950	1.29424	1.26863	1.27485	1.02078	0.324	O'Donovan et al. (2007)
WASP-12b	0.02290	1002.7	1.7900	1.78180	1.62438	1.65677	1.10196	0.552	Hebb et al. (2009)
OGLE-TR-113b	0.02290	618.9	1.0900	1.08963	1.07427	1.07804	1.01464	0.287	Gillon et al. (2006)
WASP-4b	0.02300	840.5	1.4160	1.41410	1.35814	1.37110	1.04260	0.410	Southworth et al. (2009b)
CoRoT-1b	0.02540	966.0	1.4900	1.48811	1.42950	1.44307	1.04232	0.409	Barge et al. (2008)
WASP-5b	0.02729	653.2	1.1710	1.17072	1.15789	1.16106	1.01132	0.263	Southworth et al. (2009c)
CoRoT-2b	0.02810	306.9	1.4650	1.46465	1.45111	1.45447	1.00958	0.251	Alonso et al. (2008)
GJ 436b	0.02872	6574.8	0.4380	0.43798	0.43578	0.43633	1.00510	0.199	Bean et al. (2008)
SWEPS-11	0.03000	118.8	1.1300	1.12997	1.12842	1.12881	1.00140	0.134	Sahu et al. (2006)
OGLE-TR-132b	0.03060	1157.6	1.1800	1.17968	1.16311	1.16716	1.01453	0.285	Gillon et al. (2007)
HD 189733b	0.03099	741.5	1.1380	1.13784	1.12891	1.13112	1.00806	0.235	Bouchy et al. (2005)
WASP-2b	0.03138	962.5	1.0170	1.01689	1.00975	1.01152	1.00718	0.225	Daemgen et al. (2009)
WASP-3b	0.03170	737.9	1.3100	1.30970	1.29521	1.29878	1.01142	0.264	Gibson et al. (2008)
TrES-2	0.03556	856.0	1.2720	1.27181	1.26116	1.26380	1.00859	0.240	Daemgen et al. (2009)
XO-2b	0.03690	1800.6	0.9730	0.97291	0.96602	0.96773	1.00723	0.225	Burke et al. (2007)
WASP-14b	0.03700	178.8	1.2590	1.25897	1.25705	1.25753	1.00155	0.138	Joshi et al. (2008)
WASP-10b	0.03710	243.0	1.0800	1.07998	1.07858	1.07893	1.00132	0.130	Johnson et al. (2009)
HAT-P-7b	0.03790	855.3	1.4210	1.42075	1.40709	1.41046	1.00988	0.251	Welsh et al. (2010)
WASP-1b	0.03820	1459.2	1.3580	1.35766	1.33881	1.34342	1.01433	0.283	Cameron et al. (2007)
HAT-P-12b	0.03840	3623.4	0.9590	0.95886	0.94733	0.95015	1.01232	0.268	Hartman et al. (2009)
HAT-P-3b	0.03894	1636.5	0.8900	0.88996	0.88621	0.88714	1.00428	0.189	Torres et al. (2007)
TrES-1	0.03930	1493.7	1.0810	1.08090	1.07369	1.07548	1.00681	0.221	Alonso et al. (2004)
HAT-P-5b	0.04075	1146.1	1.2600	1.25986	1.25071	1.25298	1.00742	0.228	Bakos et al. (2007a)
OGLE-TR-10b	0.04162	1961.6	1.2600	1.25978	1.24518	1.24877	1.01190	0.266	Pont et al. (2007)
WASP-6b	0.04210	2456.9	1.2240	1.22377	1.20807	1.21191	1.01319	0.275	Gillon et al. (2009)
WASP-16b	0.04210	1251.9	1.0080	1.00796	1.00422	1.00515	1.00377	0.181	Lister et al. (2009)
HAT-P-13b	0.04260	1501.4	1.2800	1.27983	1.26869	1.27144	1.00892	0.242	Bakos et al. (2009a)
HD 149026b	0.04313	3792.5	0.6540	0.65399	0.65211	0.65258	1.00289	0.165	Sato et al. (2005)
HAT-P-10b	0.04390	1867.0	1.0450	1.04493	1.03927	1.04068	1.00551	0.205	Bakos et al. (2009b)

Table 2: Continuation of Table 1.

name	a	q	Rsub	Rback	Rpole	Rside	rr	f_i	Reference
HAT-P-4b	0.04460	1940.6	1.2700	1.26983	1.25768	1.26067	1.00980	0.249	Kovacs et al. (2007)
XO-3b	0.04540	107.8	1.2170	1.21699	1.21644	1.21658	1.00046	0.092	Johns-Krull et al. (2008)
Lupus-TR-3b	0.04640	1124.9	0.8900	0.88999	0.88845	0.88884	1.00174	0.140	Weldrake et al. (2008)
OGLE-TR-111b	0.04700	1620.4	1.0670	1.06695	1.06259	1.06367	1.00415	0.187	Pont et al. (2004)
HD 209458b	0.04707	1544.2	1.3200	1.31987	1.31023	1.31262	1.00746	0.228	Henry et al. (2000)
XO-5b	0.04870	855.7	1.0890	1.08898	1.08672	1.08728	1.00210	0.150	Burke et al. (2008)
HAT-P-8b	0.04870	882.0	1.5000	1.49987	1.49157	1.49364	1.00565	0.208	Latham et al. (2009)
XO-1b	0.04880	1163.7	1.1840	1.18395	1.17970	1.18076	1.00364	0.179	McCullough et al. (2006)
CoRoT-5b	0.04947	2242.6	1.3880	1.38780	1.37313	1.37674	1.01083	0.257	Rauer et al. (2009)
WASP-15b	0.04990	2280.1	1.4280	1.42777	1.41152	1.41551	1.01168	0.264	West et al. (2009)
TrES-4	0.05091	1577.2	1.7990	1.79853	1.77205	1.77851	1.01521	0.289	Daemgen et al. (2009)
OGLE-TR-211b	0.05100	1352.4	1.3600	1.35990	1.35240	1.35427	1.00562	0.207	Udalski et al. (2008)
OGLE-TR-182b	0.05100	1182.1	1.1300	1.12997	1.12682	1.12761	1.00282	0.165	Pont et al. (2008)
WASP-17b	0.05100	2564.9	1.7400	1.73935	1.70224	1.71115	1.02218	0.327	Anderson et al. (2010)
HAT-P-6b	0.05235	1278.2	1.3300	1.32993	1.32392	1.32541	1.00459	0.194	Noyes et al. (2008)
WASP-13b	0.05270	2937.0	1.2100	1.20990	1.20067	1.20295	1.00777	0.230	Skillen et al. (2009)
HAT-P-9b	0.05300	1718.7	1.4000	1.39988	1.39036	1.39272	1.00694	0.222	Shporer et al. (2009)
HAT-P-11b	0.05300	10473.2	0.4520	0.45200	0.45136	0.45152	1.00142	0.129	Bakos et al. (2009c)
SWEEPS-04	0.05500	341.8	0.8100	0.81000	0.80981	0.80985	1.00024	0.073	Sahu et al. (2006)
HAT-P-1b	0.05530	2264.5	1.2250	1.22493	1.21844	1.22005	1.00539	0.204	Bakos et al. (2007b)
XO-4b	0.05550	803.8	1.3400	1.33996	1.33668	1.33750	1.00248	0.158	McCullough et al. (2008)
CoRoT-3b	0.05700	66.2	1.0100	1.01000	1.00992	1.00994	1.00008	0.052	Deleuil et al. (2008)
WASP-7b	0.06180	1396.4	0.9150	0.91499	0.91409	0.91432	1.00099	0.116	Hellier et al. (2009)
HAT-P-2b	0.06878	156.7	1.1570	1.15700	1.15681	1.15686	1.00016	0.065	Pál et al. (2009)
WASP-8b	0.07930	638.7	1.1700	1.17000	1.16947	1.16961	1.00045	0.090	Smith et al. (2009)
CoRoT-6b	0.08550	373.3	1.1660	1.16600	1.16576	1.16582	1.00021	0.070	Fridlund et al. (2010)
CoRoT-4b	0.09000	1600.1	1.1900	1.18999	1.18904	1.18928	1.00081	0.108	Moutou et al. (2008)
HD 17156b	0.16230	404.3	1.0230	1.02300	1.02298	1.02298	1.00002	0.033	Winn et al. (2009)
HD 80606b	0.44900	239.2	1.0290	1.02900	1.02900	1.02900	1.00000	0.010	Fossey et al. (2009)

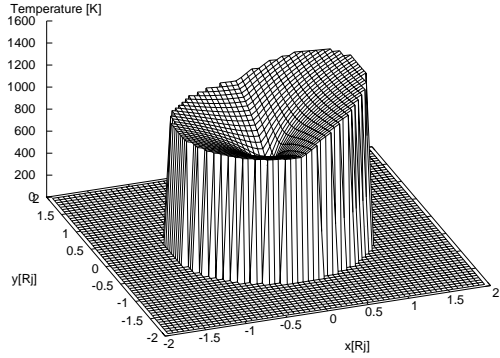


Fig. 1.— A 2D projection map of the surface temperature of HD189733b calculated for $P_r = 0.6$, $P_a = 0.1$. x-axis points to the star, z-axis to the rotation pole. One can clearly see the hot region on the day side of the planet facing the star. The night side has a non zero temperature due to the efficient heat redistribution ($P_r = 0.6$). The temperature at the polar region, $(x, y) = (0, 0)$, drops significantly since the heat is redistributed efficiently along parallels but much less effectively along the meridians ($P_a = 0.1$).

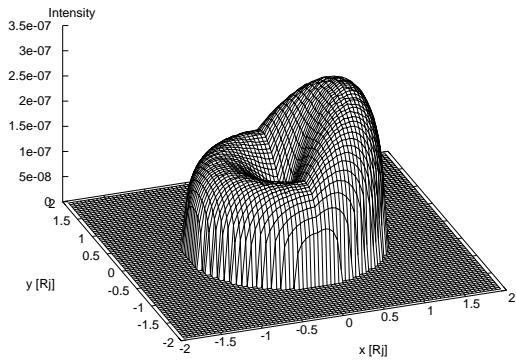


Fig. 2.— A 2D projection image of HD189733b at 8 micron seen pole-on. The surface intensity is in $erg/s/Hz/cm^2/sterad$. It corresponds to the temperate distribution from Fig.1. The limb darkening ($u_1 = 0.6, u_2 = 0.2$) was applied to it. Notice that hot regions are now actually dark due to the limb darkening.

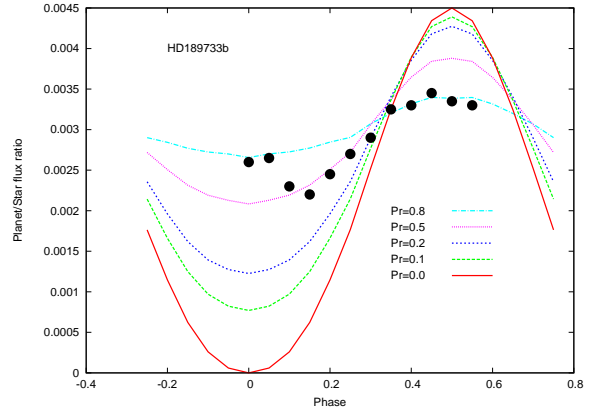


Fig. 3.— Theoretical light-curves of HD189733b compared with the observations of Knutson et al.(1997) at 8 micron (black circles). Observe the strong dependence on the heat redistribution parameter P_r which could reach several orders of magnitude at phase zero. $A_B = 0, P_a = 1.0$, and zero limb darkening were assumed.

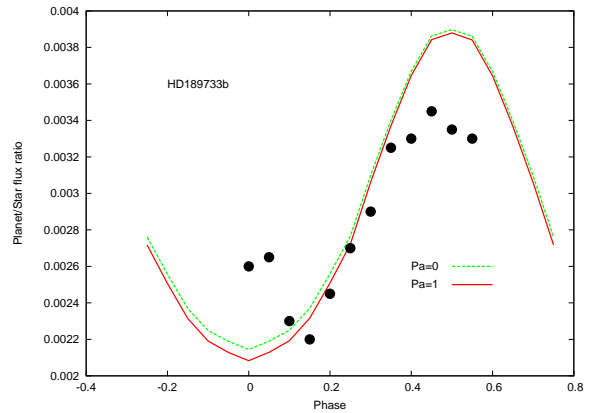


Fig. 4.— The effect of the zonal temperature distribution on the light-curve of transiting exoplanet HD189733b at 8 micron. If the heat flows mainly along the parallels and not along meridians ($P_a = 0$) then one would detect slightly more light at all phases, especially on the night side. Black circles are the observations of Knutson et al.(1997). $A_B = 0, P_r = 0.5$, and zero limb darkening were assumed.

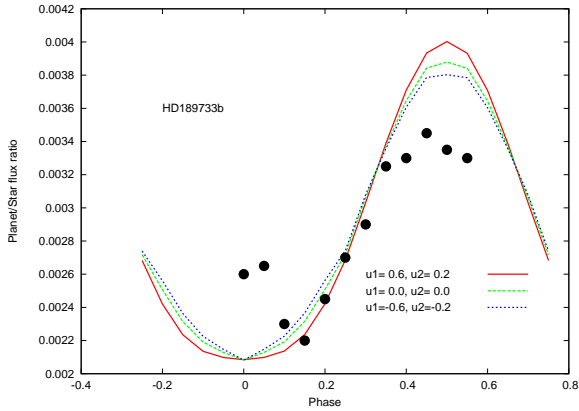


Fig. 5.— The effect of the limb darkening on the theoretical light-curve of the transiting exoplanet HD189733b at 8 micron. Limb darkening has almost no effect at phase zero but much stronger effect shortly before and after the transit and near the secondary eclipse. This is because when we observe the night side with almost constant temperature distribution the darkening at the limb is compensated by the brightening at the center to conserve the flux. However, during the secondary eclipse the limb darkening suppresses the radiation from the cold regions and amplifies the radiation from the hot regions. The net effect is that planet is brighter at the phase 0.5. The opposite happens shortly before and after the transit. The possible limb brightening would have the opposite behaviour. Black circles are the observations of Knutson et al.(1997). $A_B = 0$, $P_r = 0.5$, $P_a = 1.0$ were assumed.

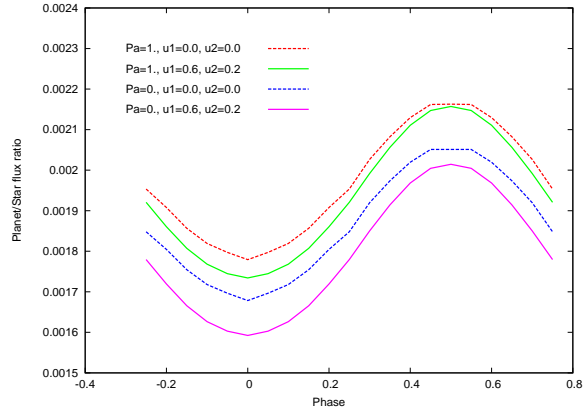


Fig. 6.— The effect of the temperature distribution (P_a parameter) and limb darkening on the light-curve of a hypothetical exoplanet seen at small inclination of 20 degrees. Contrary to the case with homogeneous temperature distribution ($P_a = 1$), one would observe less flux from the models with the dominant east-west heat circulation ($P_a = 0$) since the polar regions visible at this inclination are quite cool. Limb darkening would dim the hotter equatorial regions even further and reduce the observed flux, especially for models with the dominant east-west heat circulation ($P_a = 0$). $A_B = 0$, $P_r = 0.5$ were assumed.

